LETTER

doi:10.1038/nature10522

Rad51 paralogues Rad55–Rad57 balance the antirecombinase Srs2 in Rad51 filament formation

Jie Liu[1], Ludovic Renault[2], Xavier Veaute[3], Francis Fabre[3], Henning Stahlberg[2,4] & Wolf-Dietrich Heyer[1,2]

Homologous recombination is a high-fidelity DNA repair pathway. Besides a critical role in accurate chromosome segregation during meiosis, recombination functions in DNA repair and in the recovery of stalled or broken replication forks to ensure genomic stability. In contrast, inappropriate recombination contributes to genomic instability, leading to loss of heterozygosity, chromosome rearrangements and cell death. The RecA/UvsX/RadA/Rad51 family of proteins catalyses the signature reactions of recombination, homology search and DNA strand invasion[1,2]. Eukaryotes also possess Rad51 paralogues, whose exact role in recombination remains to be defined[3]. Here we show that the *Saccharomyces cerevisiae* Rad51 paralogues, the Rad55–Rad57 heterodimer, counteract the antirecombination activity of the Srs2 helicase. The Rad55–Rad57 heterodimer associates with the Rad51–single-stranded DNA filament, rendering it more stable than a nucleoprotein filament containing Rad51 alone. The Rad51–Rad55–Rad57 co-filament resists disruption by the Srs2 antirecombinase by blocking Srs2 translocation, involving a direct protein interaction between Rad55–Rad57 and Srs2. Our results demonstrate an unexpected role of the Rad51 paralogues in stabilizing the Rad51 filament against a biologically important antagonist, the Srs2 antirecombination helicase. The biological significance of this mechanism is indicated by a complete suppression of the ionizing radiation sensitivity of *rad55* or *rad57* mutants by concomitant deletion of *SRS2*, as expected for biological antagonists. We propose that the Rad51 presynaptic filament is a meta-stable reversible intermediate, whose assembly and disassembly is governed by the balance between Rad55–Rad57 and Srs2, providing a key regulatory mechanism controlling the initiation of homologous recombination. These data provide a paradigm for the potential function of the human RAD51 paralogues, which are known to be involved in cancer predisposition and human disease.

Rad51 protein and its homologues RecA, UvsX and RadA form nucleoprotein filaments with ssDNA that perform homology search and DNA strand invasion during homologous recombination. The Rad51 paralogues share the RecA core with the Rad51 protein featuring unique amino- and carboxy-terminal extensions (Supplementary Fig. 2), but themselves do not form filaments and are unable to perform homology search and DNA strand invasion[2–4]. Whereas humans contain five paralogues (RAD51B, RAD51C, RAD51D, XRCC2, XRCC3), the budding yeast *Saccharomyces cerevisiae* contains two clearly identifiable paralogues, Rad55 and Rad57 (Supplementary Fig. 2). Rad55 and Rad57 in yeast as well as the five human RAD51 paralogues have unique non-redundant functions in recombination, and mutations in any one of them lead to recombination defects, chromosomal instability, sensitivity to DNA damage, and meiotic defects[1–3]. Defects in the budding yeast *RAD55* and *RAD57* genes lead to identical and epistatic phenotypes in DNA repair and recombination, consistent with the formation of a stable Rad55–Rad57 heterodimer[4,5]. Rad55–Rad57 heterodimers were inferred to function as mediator proteins[6] allowing assembly of the Rad51 nucleoprotein filament on ssDNA covered by the eukaryotic ssDNA-binding protein RPA[4]. This suggested that Rad55–Rad57 are involved in the nucleation of the Rad51 filament, which is otherwise inhibited on RPA-covered ssDNA. This nucleation model is akin to the role of RecFOR or BRCA2 in nucleating RecA or human RAD51 filaments[7–9]. Rad51 filament formation *in vivo* can be monitored cytologically as Rad51 focus formation at the site of DNA damage[10]. Unexpectedly, Rad51 focus formation after ionizing radiation in yeast was demonstrated to be independent of Rad55–Rad57 and formation of visible Rad55–Rad57 foci required Rad51 (ref. 10). These results are difficult to reconcile with the nucleation model derived from the biochemical results and suggest an alternative function of Rad55–Rad57 *in vivo*.

To address the function of the Rad51 paralogues in yeast, we determined the effect of Rad55–Rad57 on the stability of Rad51–ssDNA nucleoprotein complexes. Deletion mutants of the *RAD55* or *RAD57* genes display a curious enhancement of some phenotypes at low temperature (in particular ionizing radiation sensitivity; see Supplementary Fig. 12)[5], indicating that these proteins are involved in the stabilization of a molecular complex, probably the Rad51 presynaptic filament. To test this hypothesis, we incubated subsaturating amounts of Rad51 protein with ssDNA (1 Rad51 per 15 nucleotides) in the presence of substoichiometric amounts of Rad55–Rad57 heterodimer (1 Rad55–Rad57 per 4 Rad51) and challenged the filaments with buffer containing a high salt concentration (500 mM NaCl) (Supplementary Fig. 3a, b). Under these conditions, Rad51 does not maintain stable complexes with ssDNA during electrophoresis. However, the presence of Rad55–Rad57 resulted in stable, Rad51-containing ssDNA complexes that withstood the salt challenge. In a complementary approach, we examined the effect of Rad55–Rad57 on Rad51 filament formation at near-physiological ionic strength (90 mM NaCl) (Fig. 1a, b). Under these conditions, only a fraction of the available Rad51 binds ssDNA, causing retarded mobility of the DNA (Fig. 1b, lane 3). Addition of substoichiometric amounts of Rad55–Rad57 (1 Rad55–Rad57 per 6 Rad51 in lane 4 of Fig. 1b) led to the formation of a novel, supershifted complex that contained both Rad51 and Rad55–Rad57, as demonstrated by immunoblotting. Rad55–Rad57 heterodimer alone binds to DNA under these conditions, leading to the formation of protein networks that are too large to enter the gel (Fig. 1b, lane 2). The results from both experiments (Fig. 1b; Supplementary Fig. 3) indicate that Rad55–Rad57 form a co-complex with Rad51 on ssDNA and stabilize Rad51–ssDNA filaments. Indeed, immunogold electron microscopy targeted towards Rad55 (glutathione *S*-transferase (GST)-tag; see Fig. 1c) directly visualized Rad55 associated with the Rad51–ssDNA filaments (Fig. 1d). Control experiments demonstrated the specificity of the gold labelling (Supplementary Table 1) with over 90% of the gold particles associated with clearly identifiable Rad51 filaments. The remainder may have associated with filaments too short to be scored or with free Rad55–Rad57. Gold particles were found either at the filament terminus ($n = 40$) or

[1]Department of Microbiology, University of California, Davis, Davis, California 95616-8665, USA. [2]Department of Molecular & Cellular Biology, University of California, Davis, Davis, California 95616-8665, USA. [3]CEA-DSV-Institut de Radiobiologie Cellulaire et Moléculaire, UMR217 CNRS/CEA, F-92265 Fontenay aux Roses, France. [4]Center for Cellular Imaging and Nanoanalytics, University Basel, CH-4056 Basel, Switzerland.

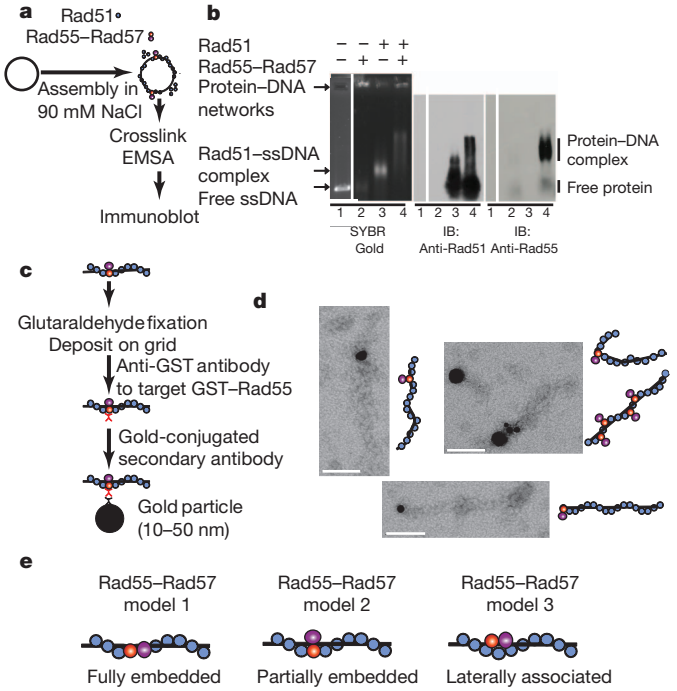

Figure 1 | Rad55–Rad57 is associated with and stabilizes Rad51–ssDNA filaments. **a**, Rad51–ssDNA filament assembly assay. EMSA, electrophoretic mobility shift assay. **b**, Rad51 (0.67 μM) with or without Rad55–Rad57 (0.11 μM) was incubated with 4 μM ϕX174 ssDNA. The migration position of free protein was confirmed in controls lacking DNA (Supplementary Fig. 3c). IB, immunoblot. **c**, Reaction scheme of immunoaffinity gold labelling of Rad55. **d**, Electron microscopy images of gold-labelled Rad55 associated with Rad51–ssDNA filament (1:3 Rad51:nucleotide; 2.34 μM Rad51 ± 0.43 μM Rad55–Rad57, 7 μM ssDNA). Scale bars, 100 nm. **e**, Models for the disposition of Rad55–Rad57 with the Rad51 filament. For simplicity, only model 2 is drawn in further illustrations.

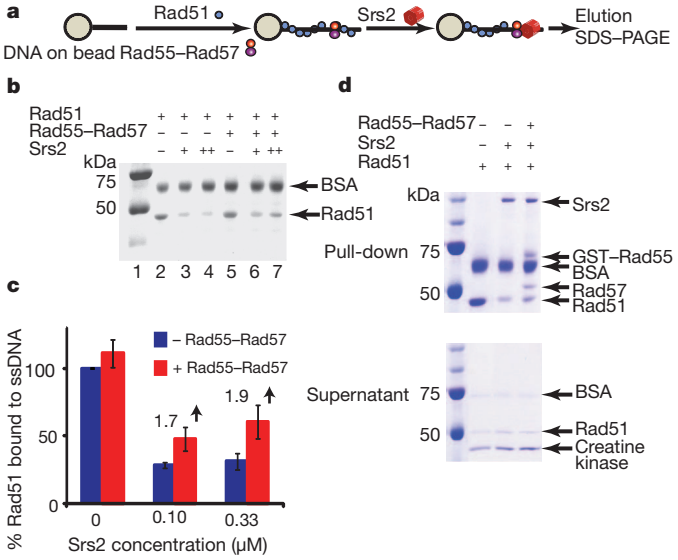

Figure 2 | Rad55–Rad57 stabilize Rad51–ssDNA filaments to resist disruption by Srs2. **a**, Pull-down assay measuring stability of Rad51–ssDNA complexes (1:3 Rad51:nucleotide, 1 μM Rad51 ± 0.1 μM Rad55–Rad57) against disruption by Srs2 (0.1 or 0.33 μM). **b**, Rad51 remaining bound to ssDNA. **c**, Quantification of results in **b** and additional experiments. Shown are means ± 1 s.d., $n = 3$. **d**, Concomitant binding of Rad55–Rad57 and Srs2 to Rad51-covered ssDNA. Pull-down assay measuring stability of Rad51–ssDNA complexes (1:3 Rad51:nucleotide, 1 μM Rad51 ± 0.2 μM Rad55–Rad57) against disruption by 0.33 μM Srs2. Top, pull-downs; bottom, supernatants.

interstitially ($n = 43$) (Supplementary Table 1). Negative controls with Rad51 filaments assembled in the absence of Rad55–Rad57 showed negligible gold labelling (Supplementary Table 1). These data show that Rad55–Rad57 are associated with the Rad51–ssDNA filament, but the exact disposition of the heterodimer with the filament remains to be determined (see Fig. 1e).

Salt stability of protein–DNA complexes is a valuable biochemical criterion. To establish biological significance, we tested whether Rad55–Rad57 heterodimers stabilize Rad51–ssDNA filaments against a biologically relevant destabilizer. The Srs2 helicase was identified as a negative regulator of homologous recombination, and genetic experiments indicated that Srs2 targets Rad51 protein[11–13]. Consistent with the genetic data, Srs2 translocates on ssDNA and disrupts Rad51 presynaptic filaments *in vitro*, providing a compelling mechanism for its function as an antirecombinase[14–16]. In the presence of 0.1 or 0.33 μM Srs2 approximately 70% of the Rad51 is dissociated as assessed by measuring Rad51 associated with ssDNA coupled to magnetic beads (Fig. 2a–c). The presence of substoichiometric amounts of Rad55–Rad57 (0.1 μM) enhanced the recovery of ssDNA-bound Rad51 by ~twofold (from 31% to 60% in the presence of 0.33 μM Srs2). Rad55–Rad57 and Srs2 bound to Rad51-covered ssDNA in a quantitative and concomitant manner (Fig. 2d). Together the data show that Rad55–Rad57 inhibit Srs2 when bound to DNA and not in solution. Concentration-dependent inhibition of Srs2-mediated dissociation of Rad51 from ssDNA by Rad55–Rad57 was also observed in a topology-based assay (Supplementary Figs 4, 5).

To investigate the role of Rad55–Rad57 in antagonizing disruption of Rad51 presynaptic filaments by Srs2 further, we used electron microscopy to examine nucleoprotein filaments directly (Fig. 3 and Supplementary Fig. 6). Rad51 filaments were assembled on a 600-nucleotide fragment of ssDNA and RPA was added to visualize free ssDNA. Consistent with previous observations[14,15], in the absence of Rad55–Rad57 Srs2 disrupts the Rad51–ssDNA filament efficiently, leading to binding of RPA to the newly exposed ssDNA (Fig. 3). Importantly, when substoichiometric amounts of Rad55–Rad57 were incubated with Rad51 and ssDNA, the filaments were stabilized against disruption by Srs2, as indicated by the significantly increased mean filament length.

How do Rad55–Rad57 heterodimers block Srs2 from dissociating Rad51 from ssDNA? Srs2 is known to interact with Rad51 and trigger the Rad51 ATPase leading to dissociation of Rad51 from ssDNA[16]. We found that Rad55–Rad57 form a 1:1 complex with Srs2 (Fig. 4a) and have higher affinity to Srs2 than to Rad51 (Fig. 4b, c). Excess Rad51 does not compete with Srs2 binding to Rad55–Rad57 (Supplementary Fig. 7). Moreover, Rad55–Rad57 heterodimers are able to simultaneously bind Rad51 and Srs2 in a 1:1:1 stoichiometry (Fig. 4d and Supplementary Figs 7–9). We considered the possibility that Rad55–Rad57 inhibit the Srs2 ATPase activity and by that Srs2 translocation, but Srs2 ATPase activity is barely altered by the presence of Rad55–Rad57 (data not shown). Srs2 translocase/helicase activity is stimulated by Rad51 binding to DNA[17] (Fig. 4e–g). Importantly, Rad55–Rad57 completely suppress this stimulatory effect of Rad51, leading to inhibition of the Srs2 helicase activity even at a fivefold molar excess of Srs2 over Rad55–Rad57 (Fig. 4f, g and Supplementary Fig. 10). This substoichiometric action of Rad55–Rad57 eliminates the possibility that Rad55–Rad57 inhibition functions by binding Srs2 in solution. Rad55–Rad57 only slightly inhibit Srs2 helicase in the absence of Rad51 (Fig. 4g and Supplementary Fig. 10c). Control experiments show that this effect depends on Srs2 translocating in the expected 3′ to 5′ direction (Supplementary Fig. 10d), showing that Rad55–Rad57 inhibit Srs2 translocation on DNA to increase filament stability (Figs 1 and 2) and function (Supplementary Fig. 11). Direct visualization of human RAD51 filaments revealed that RAD51 is only able to form discontinuous short clusters on double-stranded DNA, as a result of frequent nucleation but limited extension[18,19]. If this property holds

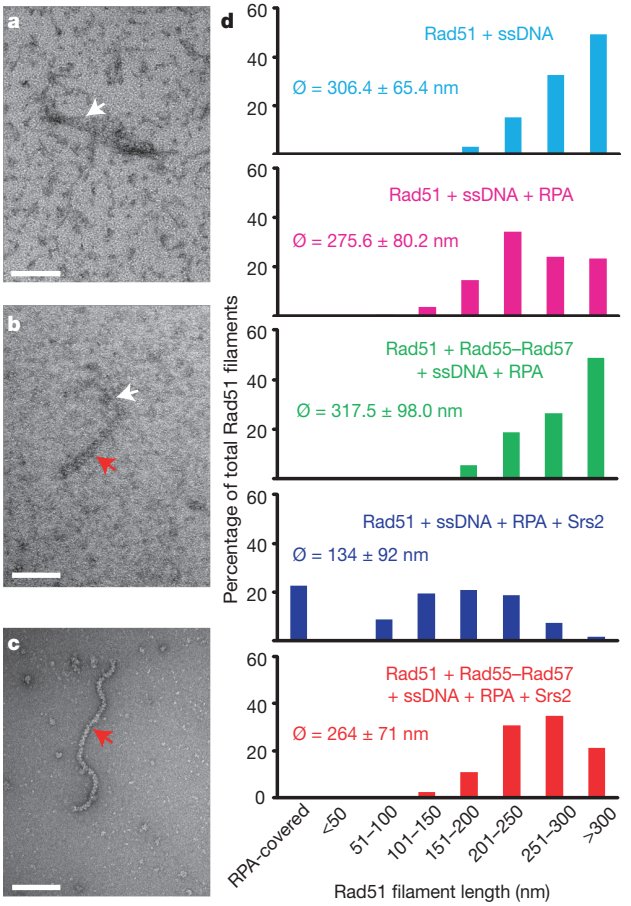

Figure 3 | Rad55–Rad57 inhibit disruption of Rad51 presynaptic filaments by Srs2. **a**, RPA–ssDNA complex. **b**, Short (145 nm) Rad51–ssDNA filament. **c**, Long (350 nm) Rad51–ssDNA filaments. **d**, Quantification of electron microscopic analysis. For each reaction condition 300–400 filaments were analysed (2.34 μM Rad51, 7 μM 600-nucleotide ssDNA, ± 0.43 μM Rad55–Rad57, ± 0.21 μM RPA, ± 0.4 μM Srs2), and the means (ø) ± 1 s.d. and distributions of filament length classes are shown. Scale bars, 100 nm. White arrows indicate RPA–ssDNA complexes and red arrows indicate Rad51 filaments.

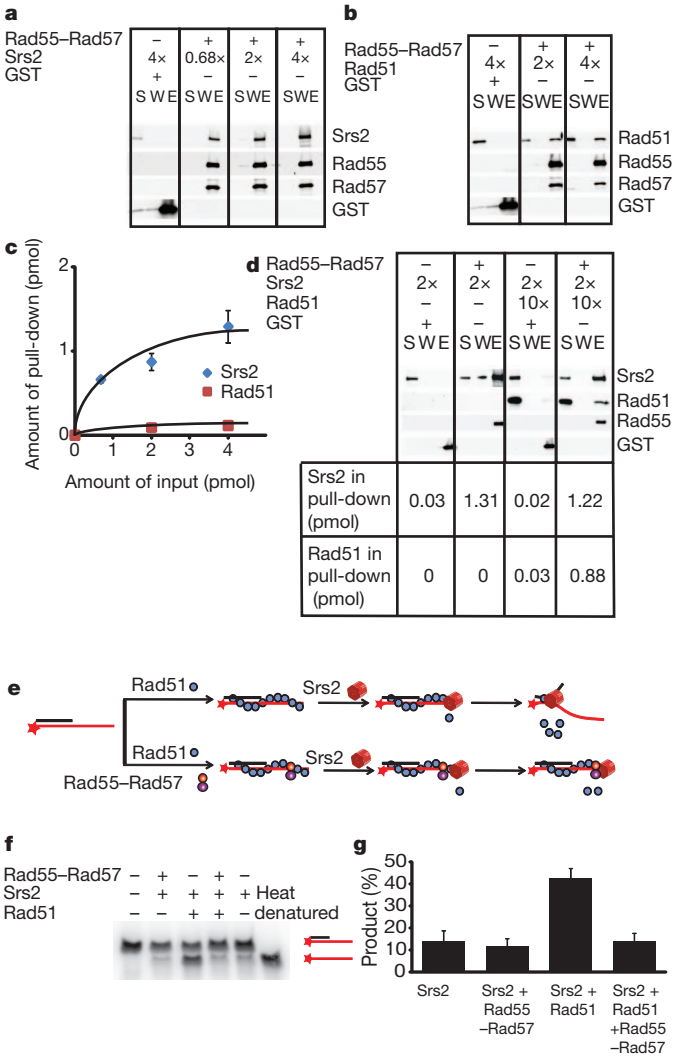

Figure 4 | Rad55–Rad57 interact with Srs2 and inhibit Srs2 helicase. **a**, Pull-down with 4 nM (1 pmol) Rad55–Rad57 and 2.7, 8, or 16 nM Srs2. **b**, Pull-down with 4 nM Rad55–Rad57 and 8 or 16 nM Rad51. **c**, Quantification of results in **a** and **b** and additional experiments. **d**, Pull-down with 4 nM Rad55–Rad57 and 8 nM Srs2 ± 40 nM Rad51. GST was used as control. S, supernatant; W, wash; E, eluate. **e**, Helicase assay. **f**, Rad51 (28 nM) with or without Rad55–Rad57 (25 nM) were incubated with 1.5 nM 3′-tailed substrate before addition of 120 nM Srs2 protein. **g**, Product yields at 20 min. Means ± 1 s.d., $n = 3$, are shown.

true for ssDNA, the formation of a co-filament with Rad51 by Rad55–Rad57 might provide a mechanism to form extended Rad51 filaments. This could also explain the increase in Rad55–Rad57 focus intensity over time after ionizing radiation exposure, and is consistent with the dependence of Rad55–Rad57 foci on Rad51 (ref. 10).

Our biochemical data are consistent with a model (Supplementary Fig. 1) whereby Rad51 presynaptic filament formation is modulated by a balance between the stabilizing function of Rad55–Rad57 and the destabilizing function of Srs2 antirecombinase. This model predicts that a deletion of *SRS2* should suppress the phenotypes caused by defects in Rad55–Rad57. In fact, *srs2Δ* completely suppresses the ionizing radiation sensitivity of *rad57* and *rad55* mutations in quantitative survival assays (Supplementary Fig. 12), consistent with semiquantitative results using *rad57* (ref. 20). However, *srs2Δ* only mildly suppresses the methyl methanesulphonate sensitivity (Supplementary Fig. 13) and recombination defect (Supplementary Fig. 14) of a *rad55* mutation, consistent with previous *rad57* data[20]. The difference in suppression is likely related to a difference in substrates: ionizing radiation-induced DNA damage requires primarily double-strand break repair, whereas methyl methanesulphonate-induced DNA damage and sister chromatid recombination require gap repair (Supplementary Fig. 1). We propose that the Rad51 presynaptic filament is a meta-stable reversible intermediate, whose dynamics in yeast are partially controlled by the balance of the filament-stabilizing activity of Rad55–Rad57 and the filament-destabilizing activity of the Srs2 helicase (Supplementary Fig. 1). This balance is likely to be influenced by the multiple post-translational modifications that have been identified to regulate Rad55–Rad57 (ref. 21) and Srs2 (ref. 22) functions (Supplementary Fig. 1)[1]. Together with the local availability of SUMO–PCNA, which specifically recruits Srs2 (refs [23–25]), post-translational modifications may determine the balance between recombination and antirecombination in wild-type cells and explain the various degrees of suppression observed in the *srs2 rad55 (rad57)* double mutants that depend on the type of DNA damage or genetic endpoint (double-strand break versus replication-fork-associated gap in Supplementary Fig. 1).

The human RAD51 paralogues have important roles in tumour suppression and human disease[3,26]. Our studies established an unprecedented mechanism of anti-antirecombination that may serve as a

paradigm for the mechanism of action of the five human RAD51 paralogues. The diversification of the human RAD51 paralogues may reflect the multiplicity of human motor proteins that may disrupt RAD51 presynaptic filaments, including the RecQ-like helicases BLM and RECQL5 as well as FBH1 and FANCJ[27–30] or indicate additional functions during recombinational repair.

METHODS SUMMARY

Purification of yeast Rad51, Rad55–Rad57, RPA and Srs2, the biochemical assays and the electron microscopy analysis are detailed in Methods.

Full Methods and any associated references are available in the online version of the paper at www.nature.com/nature.

Received 25 September 2009; accepted 30 August 2011.
Published online 23 October 2011.

1. Heyer, W. D., Ehmsen, K. T. & Liu, J. Regulation of homologous recombination in eukaryotes. *Annu. Rev. Genet.* **44,** 113–139 (2010).
2. Symington, L. S. Role of *RAD52* epistasis group genes in homologous recombination and double-strand break repair. *Microbiol. Mol. Biol. Rev.* **66,** 630–670 (2002).
3. Thacker, J. The *RAD51* gene family, genetic instability and cancer. *Cancer Lett.* **219,** 125–135 (2005).
4. Sung, P. Yeast Rad55 and Rad57 proteins form a heterodimer that functions with replication protein A to promote DNA strand exchange by Rad51 recombinase. *Genes Dev.* **11,** 1111–1121 (1997).
5. Lovett, S. T. & Mortimer, R. K. Characterization of null mutants of the *RAD55* gene of *Saccharomyces cerevisiae*: effects of temperature, osmotic strength and mating type. *Genetics* **116,** 547–553 (1987).
6. Beernink, H. T. H. & Morrical, S. W. RMPs: recombination/replication mediator proteins. *Trends Biochem. Sci.* **24,** 385–389 (1999).
7. Morimatsu, K. & Kowalczykowski, S. C. RecFOR proteins load RecA protein onto gapped DNA to accelerate DNA strand exchange: a universal step of recombinational repair. *Mol. Cell* **11,** 1337–1347 (2003).
8. Liu, J., Doty, T., Gibson, B. & Heyer, W. D. Human BRCA2 protein promotes RAD51 filament formation on RPA-covered single-stranded DNA. *Nature Struct. Mol. Biol.* **17,** 1260–1262 (2010).
9. Jensen, R. B., Carreira, A. & Kowalczykowski, S. C. Purified human BRCA2 stimulates RAD51-mediated recombination. *Nature* **467,** 678–683 (2010).
10. Lisby, M., Barlow, J. H., Burgess, R. C. & Rothstein, R. Choreography of the DNA damage response: spatiotemporal relationships among checkpoint and repair proteins. *Cell* **118,** 699–713 (2004).
11. Schiestl, R. H., Prakash, S. & Prakash, L. The *SRS2* suppressor of *rad6* mutations of *Saccharomyces cerevisiae* acts by channeling DNA lesions into the *RAD52* DNA repair pathway. *Genetics* **124,** 817–831 (1990).
12. Aboussekhra, A. *et al. RADH*, a gene of *Saccharomyces cerevisiae* encoding a putative DNA helicase involved in DNA repair. Characteristics of *radH* mutants and sequence of the gene. *Nucleic Acids Res.* **17,** 7211–7219 (1989).
13. Aguilera, A. & Klein, H. L. Genetic control of intrachromosomal recombination in *Saccharomyces cerevisiae*. I. Isolation and genetic characterization of hyper-recombination mutations. *Genetics* **119,** 779–790 (1988).
14. Krejci, L. *et al.* DNA helicase Srs2 disrupts the Rad51 presynaptic filament. *Nature* **423,** 305–309 (2003).
15. Veaute, X. *et al.* The Srs2 helicase prevents recombination by disrupting Rad51 nucleoprotein filaments. *Nature* **423,** 309–312 (2003).
16. Antony, E. *et al.* Srs2 disassembles Rad51 filaments by a protein-protein interaction triggering ATP turnover and dissociation of Rad51 from DNA. *Mol. Cell* **35,** 105–115 (2009).
17. Dupaigne, P. *et al.* The Srs2 helicase activity is stimulated by Rad51 filaments on dsDNA: implications for crossover incidence during mitotic recombination. *Mol. Cell* **29,** 243–254 (2008).
18. Hilario, J., Amitani, I., Baskin, R. J. & Kowalczykowski, S. C. Direct imaging of human Rad51 nucleoprotein dynamics on individual DNA molecules. *Proc. Natl Acad. Sci. USA* **106,** 361–368 (2009).
19. Modesti, M. *et al.* Fluorescent human RAD51 reveals multiple nucleation sites and filament segments tightly associated along a single DNA molecule. *Structure* **15,** 599–609 (2007).
20. Fung, C. W., Mozlin, A. M. & Symington, L. S. Suppression of the double-strand-break-repair defect of the *Saccharomyces cerevisiae rad57* mutant. *Genetics* **181,** 1195–1206 (2009).
21. Herzberg, K. *et al.* Phosphorylation of Rad55 on serines 2, 8, and 14 is required for efficient homologous recombination in the recovery of stalled replication forks. *Mol. Cell. Biol.* **26,** 8396–8409 (2006).
22. Saponaro, M. *et al.* Cdk1 targets Srs2 to complete synthesis-dependent strand annealing and to promote recombinational repair. *PLoS Genet.* **6,** e1000858 (2010).
23. Papouli, E. *et al.* Crosstalk between SUMO and ubiquitin on PCNA is mediated by recruitment of the helicase Srs2p. *Mol. Cell* **19,** 123–133 (2005).
24. Pfander, B., Moldovan, G. L., Sacher, M., Hoege, C. & Jentsch, S. SUMO-modified PCNA recruits Srs2 to prevent recombination during S phase. *Nature* **436,** 428–433 (2005).
25. Burgess, R. C. *et al.* Localization of recombination proteins and Srs2 reveals anti-recombinase function *in vivo*. *J. Cell Biol.* **185,** 969–981 (2009).
26. Meindl, A. *et al.* Germline mutations in breast and ovarian cancer pedigrees establish RAD51C as a human cancer susceptibility gene. *Nature Genet.* **42,** 410–414 (2010).
27. Hu, Y. *et al.* RECQL5/Recql5 helicase regulates homologous recombination and suppresses tumor formation via disruption of Rad51 presynaptic filaments. *Genes Dev.* **21,** 3073–3084 (2007).
28. Bugreev, D. V., Yu, X., Egelman, E. H. & Mazin, A. V. Novel pro- and anti-recombination activities of the Bloom's syndrome helicase. *Genes Dev.* **21,** 3085–3094 (2007).
29. Sommers, J. A. *et al.* FANCJ uses its motor ATPase to destabilize protein-DNA complexes, unwind triplexes, and inhibit RAD51 strand exchange. *J. Biol. Chem.* **284,** 7505–7517 (2009).
30. Fugger, K. *et al.* Human Fbh1 helicase contributes to genome maintenance via pro- and anti-recombinase activities. *J. Cell Biol.* **186,** 655–663 (2009).

Supplementary Information is linked to the online version of the paper at www.nature.com/nature.

Acknowledgements We thank M. Alexeeva for the cell culture support. We thank P. Sung, R. Kolodner and L. Symington for plasmids and yeast strains. We are grateful to S. Kowalczykowski, N. Hunter, D. Castaño-Diez, P. Ringler and all members of the Heyer laboratory for discussions and comments on the manuscript. This work was supported by Postdoctoral Fellowship 17FT-0046 from the Tobacco-Related Disease Research Program (J.L.), by the European Community (LSHG-CT-2003-503303) and the Centre National de la Recherche Scientifique, the Commissariat à l'Energie Atomique (X.V., F.F.), by SystemsX.ch (H.S.), and the National Institutes of Health grants U54GM74929 (H.S.), CA92267 and GM58015 (W.-D.H.).

Author Contributions J.L. designed, performed and analysed all experiments, except the ionizing radiation survival assay, and helped write the manuscript. L.R. helped with the electron microscopy image collection and data analysis. X.V. purified the Srs2 protein. F.F. performed the ionizing radiation experiment. H.S. advised on the electron microscopy analysis. W.-D.H. conceived the project, designed experiments, coordinated collaborations, contributed to data analysis and wrote the manuscript. All authors discussed results and edited the manuscript.

Author Information Reprints and permissions information is available at www.nature.com/reprints. The authors declare no competing financial interests. Readers are welcome to comment on the online version of this article at www.nature.com/nature. Correspondence and requests for materials should be addressed to W.-D.H. (wdheyer@ucdavis.edu).

METHODS

Protein purification. Yeast Rad51, RPA and Srs2 proteins were purified as described[15,31]. The purification of Rad55–Rad57 was adapted from a previously published protocol[32]. Yeast cells overexpressing GST-Rad55–His_6–Rad57 were grown and harvested as described[32]. Cells were disrupted in Buffer B containing 10 mM Na_2HPO_4, 1.8 mM KH_2PO_4, 2.7 mM KCl, 1 M NaCl, 10% (v/v) glycerol, 10 mM β-mercaptoethanol and protease inhibitor cocktail (1 mM PMSF, 2 μM leupeptin, 1 μM pepstatin A and 1 mM benzamidine) using glass beads (0.5 mm glass beads; BioSpec Products, Inc.). The cell lysate was centrifuged at 40,000 r.p.m. for 45 min using a Ti50.2 rotor. The supernatant was collected and loaded onto a pre-equilibrated Glutathione Sepharose 4B column (GE Healthcare). After washing with buffer A (20 mM Tris-HCl pH 7.5, 1 mM EDTA, 1 M NaCl, 5 mM β-mercaptoethanol and 10% glycerol), the GST-tagged proteins were eluted with Buffer A containing 20 mM reduced glutathione plus protease inhibitor cocktail. Fractions containing the GST–Rad55–His_6–Rad57 heterodimer, as determined by 10% SDS–PAGE, were pooled and dialysed against Buffer C (50 mM NaH_2PO_4 pH 8.0, 1 M NaCl and 10% glycerol) containing the protease inhibitor cocktail. Then the pool was loaded onto a pre-equilibrated Ni-NTA agarose column and washed with Buffer C plus protease inhibitor cocktail. The bound complexes were eluted with Buffer C containing 0.5 M NaCl, 0.1 mM PMSF and 250 mM imidazole, and analysed by 10% SDS–PAGE. Fractions containing stoichiometric Rad55–Rad57 heterodimer were pooled, concentrated, dialysed into the storage buffer containing 20 mM Tris-HCl pH 7.5, 0.5 M NaCl, 0.1 mM EDTA, 1 mM DTT and 10% glycerol, and then stored in aliquots at −80 °C. The absence of contaminating enzymatic activities and DNA in protein preparations was verified as described[33].

Purification of 600-nucleotide ssDNA. As published previously[17], 600-bp dsDNA fragments biotinylated at a one 5′ end were generated by PCR from PstI-linearized ϕX174 DNA using primers WDHY427 5′-TTATCGAAGCGCGC ATAAAT-3′ and 5′ biotinylated WDHY431 5′-GTCTTCATTTCCATGCGG TG-3′. The biotinylated dsDNA was loaded onto a HiTrap Streptavidin HP column (Amersham Biosciences), and non-biotinylated single-stranded DNA was eluted with 60 mM NaOH.

Rad51–ssDNA filament assembly assay. In Fig. 1b, Rad51 (0.67 μM) was incubated with 4 μM ssDNA, in the presence or absence of 0.11 μM Rad55–Rad57, in buffer R containing 20 mM triethanolamine pH 7.5, 4 mM magnesium acetate, 2.5 mM ATP, 25 μg ml^{-1} BSA, 1 mM DTT, 90 mM NaCl and 5% glycerol for 10 min. Then 0.25% glutaraldehyde was used to crosslink the protein–DNA complexes for 15 min. The complexes were separated on a 0.5% agarose gel, stained with SYBR Gold, transferred to nitrocellulose membrane, and blotted with rabbit polyclonal anti-Rad51 or anti-Rad55 antibodies.

Rad51–ssDNA filament salt challenge assay. In Supplementary Fig. 3, Rad51 (0.267 μM) was incubated with 4 μM ssDNA, in the presence or absence of 0.067 μM Rad55–Rad57, in buffer R containing 20 mM triethanolamine pH 7.5, 4 mM magnesium acetate, 2.5 mM ATP, 25 μg ml^{-1} BSA, 1 mM DTT and 5% glycerol for 10 min. Then 5 M stock NaCl solution was added to the reaction to reach a final concentration of 500 mM for a further incubation of 30 min. Glutaraldehyde (0.25%) was used to crosslink the protein–DNA complexes for 15 min. Complexes were separated on a 0.5% agarose gel and stained with SYBR Gold. Proteins were transferred to nitrocellulose membrane and blotted with anti–Rad51 antibodies. All DNA concentrations refer to nucleotides (ssDNA) or base pairs (dsDNA).

Protein binding to ssDNA immobilized on magnetic beads. In Fig. 2b, a 5′-biotinylated oligonucleotide was immobilized onto magnetic streptavidin beads as previously described[34]. The oligo sequence is 5′-CCCCCCCCCCCCCCA AGATAATTTTTCGACTCATCAGAAATATCCGAAAGTGTTAACTTCTGCG TCATGGAAGCGATAAAACTC-3′. In experiments containing Srs2, 10-μl slurry of beads containing 3 μM ssDNA was incubated with 1 μM Rad51 in the presence and absence of 0.1 μM Rad55–Rad57 in buffer containing 20 mM triethanolamine, 5 mM magnesium acetate, 4 mM ATP, 25 μg ml^{-1} BSA, 1 mM DTT, 5% glycerol and 25 mM NaCl for 10 min at 22 °C. Then 0.1 or 0.33 μM Srs2 protein was added and further incubated for 10 min. The beads were washed, and bound proteins were eluted and quantified as described[35]. Background protein binding was typically less than 3%.

Topology-based assay for Rad51 dissociation. A published protocol was modified slightly for this assay using M13mp18 ssDNA[36]. In Supplementary Fig. 4, 375 nM Rad51, with 0, 80 and 120 nM Rad55–Rad57, were incubated with 9 μM circular M13mp18 ssDNA in 25 μl of buffer containing 20 mM triethanolamine pH 7.5, 4 mM magnesium acetate, 25 μg ml^{-1} BSA, 1 mM DTT, and an ATP-regenerating system consisting of 2.5 mM ATP, 20 U ml^{-1} creatine kinase, and 20 mM creatine phosphate for 10 min at 30 °C. Then, 100 nM Srs2 and 150 nM RPA were added and incubated for 10 min, before the addition of topologically relaxed pUC19 dsDNA (7 μM in base pairs) and wheat germ DNA topoisomerase I (3 U). After another 10 min incubation, reactions were stopped by addition of 4 μl stop solution consisting of 1% (w/v) SDS, 75 mM EDTA, 10 mg ml^{-1} protease K and further 30 min incubation at 37 °C. DNA species were resolved by electrophoresis on a 1% TBE-agarose gel and visualized using ultraviolet transillumination after ethidium bromide staining. The results were quantified using ImageQuant.

Protein interaction assays. GST–Rad55–His_6–Rad57 (4 nM) or 30 nM GST (GE Healthcare) were incubated with increasing amounts of either Srs2 or Rad51 in buffer P containing 25 mM Tris-HCl (pH 7.5), 10 mM magnesium acetate, 50 mM NaCl, 1 mM DTT, 10% glycerol and 0.05% NP-40 for 1 h at room temperature (Fig. 4a–d). Equilibrated and BSA-treated Glutathione-Sepharose 4B beads were added to the mixture and incubated for 1 h. The beads and supernatant were separated by centrifugation and the beads were washed twice with binding buffer P. The pulled-down protein complexes were eluted by boiling at 95 °C for 3 min in 10 μl SDS–PAGE loading buffer, separated through a 10% SDS–PAGE gel, and the protein bands were visualized through immunoblots and quantified by ImageQuant. In Fig. 4a, b, 1/16th of the supernatant and wash were loaded. In Fig. 4d, 1/7th of the supernatant and wash were loaded. For the competition protein binding assay (Supplementary Figs 7 and 8), the two proteins were incubated for 30 min before the addition of an increasing amount of the third challenging protein, as specified in the diagrams. After another 30-min incubation, equilibrated and BSA-treated Glutathione-Sepharose 4B beads were added to the mixture and incubated for 1 h. Analysis and quantification was performed as described above. The anti-Rad51, -Rad55 and -Rad57 antibodies were generated in rabbits, the anti-Srs2 antibody was purchased from Santa Cruz Biotechnology.

Helicase assay. The assay followed a published protocol and the substrates were prepared exactly as described before[15]. In Fig. 4f, 28 nM Rad51 with 0 or 25 nM Rad55–Rad57 were incubated with 1.5 nM oligo substrate with 3′ tail in buffer containing 20 mM triethanolamine pH 7.5, 4 mM magnesium acetate, 25 μg ml^{-1} BSA, an ATP-regenerating system consisting of 2.5 mM ATP, 20 U ml^{-1} creatine kinase and 20 mM creatine phosphate, as well as either 1 mM DTT and 40 mM NaCl (Fig. 4e, g and Supplementary Fig. 10c, d) or 5 mM DTT and 10 mM NaCl (Supplementary Fig. 10a) for 10 min at 30 °C. Then 120 nM Srs2 protein was added to initiate the helicase reaction. After 20 min incubation, the reactions were stopped by adding 4.5 μl stop buffer containing 150 mM EDTA, 2% SDS, 163 nM unlabelled oligo, and 4.3 mg ml^{-1} protease K into 9 μl reaction sample. The DNA species were separated through electrophoresis on a 10% TBE-PAGE gel, which was dried and analysed by a Storm phosphorimager. The bands were quantified by densitometry using ImageQuant.

DNA strand exchange assay. In Supplementary Fig. 11, Rad51 (3.3 μM) was incubated with 0.3 μM Rad55–Rad57 or the corresponding amount of Rad55–Rad57 storage buffer and 10 μM ϕX174 ssDNA for 15 min at 30 °C in buffer containing 30 mM Tris-acetate (pH 7.5), 4 mM magnesium acetate, 75 mM NaCl, 1 mM DTT, 2.5 mM ATP, 50 μg ml^{-1} BSA, 20 mM phosphocreatine and 80 ng $μl^{-1}$ creatine kinase. 0.56 μM RPA and 0, 333, 222, 167, 125 nM of Srs2 were added, and incubated for another 30 min. Then 10 μM (bp) PstI-linearized ϕX174 dsDNA and 4.8 mM spermidine were added and further incubated for 120 min. Samples were deproteinized and separated by electrophoresis on a 0.8% TBE-agarose gel. Images were recorded using a FluorChem8900 imaging system (Alpha Innotech) after staining with SYBR-Gold (Invitrogen), and quantified with ImageQuant. Percentage of joint molecule (JM) was calculated according to the equation JM% = (JM/1.5)/(JM/1.5 + NC + dsDNA). Percentage of product formation was calculated according to the equation product% = (JM/1.5 + NC)/(JM/1.5 + NC + dsDNA). NC, nicked circle.

Electron microscopy. To assemble the protein–DNA filament, 2.34 μM Rad51 protein, in the presence or absence of 0.43 μM Rad55–Rad57, was incubated with 7 μM 600-nt ssDNA (+) strand for 10 min at 30 °C in 20 mM triethanolamine pH 7.5, 4 mM magnesium acetate, 1 mM DTT and 3 mM ATP. RPA (0.21 μM) was added and incubated for another 10 min. Lastly, 0.4 μM Srs2 or buffer control was added and incubated for 10 min. The reaction mixtures were diluted 20-fold in 10 mM Tris-HCl pH 7.5, 50 mM NaCl and 5 mM $MgCl_2$ without chemical fixation. The samples were adsorbed onto 400 mesh carbon-coated copper grids (Ted Pella), negatively stained with 2% (w/v) uranyl acetate, blotted, and air-dried. Grids were imaged in a JEOL JEM-1230 transmission electron microscope (JEOL). Images of Rad51-filaments were randomly collected from different areas on the grid. 6–10 grids were used for each condition. Images were recorded at a nominal magnification of ×40,000 under minimum dose procedures on a Tietz 2,048 × 2,048 pixel CCD camera (TVIPS, Germany). Immunoaffinity gold labelling of GST–Rad55, as shown in Fig. 1d, was adapted from a published protocol[37]. In brief, Rad51–Rad55–Rad57–ssDNA complexes were assembled as described above and crosslinked with 0.25% glutaraldehyde for 20 min, before deposition on grids. Grids were blocked in 50 μg ml^{-1} BSA in TBST for 30 min, and then incubated with goat anti-GST antibody (GE Healthcare) for 30 min. After three 5 min washes with 50 μg ml^{-1} BSA in TBST, the grids were incubated in TBST plus a 1:5

dilution of gold particles dressed with rabbit anti-goat antibody (BioAssay Works). After two 5 min washes in 50 μg ml^{-1} BSA in TBST and one 5 min wash in 5 mM magnesium acetate, grids were stained with 2% (w/v) uranyl acetate before imaging.

***Saccharomyces cerevisiae* strains.** Strains used are listed in Supplementary Table 2.

Recombination assay. Spontaneous recombination rates between direct repeats were determined following a published fluctuation analysis protocol using the method of the median[38,39]. The direct-repeat recombination substrate has two different *ade2* alleles separated by plasmid sequences and the *URA3* gene[20]. Yeast strains were grown on YPD plates for 2 days at 30 °C for single colonies. For each strain, nine independent single colonies were randomly chosen and the entire colony was used to inoculate 4 ml YPD liquid culture. Liquid cultures were grown for 2–3 days at 30 °C to reach stationary phase. Cells were collected, washed with sterile H_2O, and suspended into 1 ml sterile H_2O. 100 μl of appropriate dilutions of each culture were spread on two plates each of SD-ADE-URA. Cells were incubated for 2 days at 30 °C. For each culture, the number of colonies on YPD were counted and totalled to determine the total cell number. The number of colonies on SD-ADE-URA were counted to determine the median number of recombinants. For each strain, recombination rates were measured independently three times and the mean values with standard deviations are shown.

MMS sensitivity assay. Yeast strains were grown overnight in liquid YPD to mid-log phase at 30 °C, and then diluted to $OD_{600\,nm} = 1$. Serial dilutions of these cell cultures were made with sterile H_2O and spotted onto YPD plates with or without methyl methanesulphonate. Plates were incubated for 3 days at 30 °C or 5 days at 22 °C before photographing using a FluorChem8900 imaging system (Alpha Innotech).

Ionizing radiation survival assay. Exponentially growing cells (1×10^7 to 2×10^7 per ml) in YPD medium at 28 °C were collected by centrifugation, washed in cold saline (0.9% NaCl), sonicated and resuspended in saline at the desired concentration. The cell suspension was γ-irradiated in a ^{137}Cs irradiator delivering 20 Gy min^{-1}. Aliquots of appropriate dilutions were spread on YPD-containing plates pre-warmed at either 23 °C or 34 °C. The plates were incubated at the corresponding temperature for 4 days (34 °C) or 6 days (23 °C) before counting the colonies. Platings were done in duplicate. The experiments were repeated at least three times, and the result of one typical assay is shown.

31. Solinger, J. A., Kiianitsa, K. & Heyer, W.-D. Rad54, a Swi2/Snf2-like recombinational repair protein, disassembles Rad51:dsDNA filaments. *Mol. Cell* **10,** 1175–1188 (2002).
32. Bashkirov, V. I., Herzberg, K., Haghnazari, E., Vlasenko, A. S. & Heyer, W. D. DNA-damage induced phosphorylation of Rad55 protein as a sentinel for DNA damage checkpoint activation in *S. cerevisiae*. *Methods Enzymol.* **409,** 166–182 (2006).
33. Zhang, X. P. & Heyer, W. D. Quality control of purified proteins involved in homologous recombination. *Methods Mol. Biol.* **745,** 329–343 (2011).
34. Mazin, A. V., Alexeev, A. A. & Kowalczykowski, S. C. A novel function of Rad54 protein - Stabilization of the Rad51 nucleoprotein filament. *J. Biol. Chem.* **278,** 14029–14036 (2003).
35. Wolner, B., van Komen, S., Sung, P. & Peterson, C. L. Recruitment of the recombinational repair machinery to a DNA double-strand break in yeast. *Mol. Cell* **12,** 221–232 (2003).
36. Schwendener, S. *et al.* Physical interaction of RECQ5 helicase with RAD51 facilitates its anti-recombinase activity. *J. Biol. Chem.* **285,** 15739–15745 (2010).
37. Van Dyck, E., Hajibagheri, N. M., Stasiak, A. & West, S. C. Visualisation of human RAD52 protein and its complexes with hRad51 and DNA. *J. Mol. Biol.* **284,** 1027–1038 (1998).
38. Lea, D. E. & Coulson, C. A. The distribution of the numbers of mutants in bacterial populations. *J. Genet.* **49,** 264–285 (1949).
39. Spell, R. M. & Jinks-Robertson, S. Determination of mitotic recombination rates by fluctuation analysis in *Saccharomyces cerevisiae*. *Methods Mol. Biol.* **262,** 3–12 (2004).